Obtaining the Equation of State for Multiphase Iron under Earth's Core Conditions using Bayesian Statistics

Run Wu[1], Shikai Xiang[2*], Yi Sun[2*], Yunting Xian[3], Yin Luo[4], Feifan Dai[5]

National Key Laboratory of Shock Wave and Detonation Physics, Institute of Fluid Physics
China Academy of Engineering Physics, Mianyang 621999, China

Key Points:

- Under the framework of Bayesian statistics, the uncertainty of parameters in the multiphase equation of state of iron is quantified.
- A simple and accurate probability method for calculating the phase boundary data of iron is proposed
- EOS estimates Earth's outer core density deficit at 8.7%-9.7% and geomagnetic power output from inner core cooling at 0.458-6.002 TW.

Plain Language Summary

Iron constitutes the primary element of the Earth's core, and understanding its thermodynamic properties is essential. The equation of state for iron is crucial for these insights. However, the inherent uncertainties in experimental data can significantly impact the parameters that define iron's equation of state. To address this, we employed Bayesian statistics coupled with Markov chain Monte Carlo (MCMC) simulations, allowing us to quantify the uncertainties surrounding these parameters. In our approach, we developed a straightforward yet effective method to calculate the probability associated with phase boundary data during the simulation process. The outcomes from our simulations yielded an equation of state that precisely mirrored a variety of experimental data sets, including phase boundary measurements, static pressure readings under diverse conditions, shock wave observations, and acoustic velocity determinations across different states. Armed with 100 posterior parameter samples, we honed in on the Earth's outer core density deficit, predicting it to fall within a range of approximately 8.7% to 9.7%. Furthermore, we estimated the geodynamo power output, generated by the latent heat released during the cooling and solidification of the Earth's inner core, to be between 0.458 and 6.002 terawatts.

Corresponding author: Shikai Xiang, `skxiang@caep.cn`

Corresponding author: Yi Sun, `ssunyyi@163.com`

Abstract

Iron is the primary constituent element of Earth's core, and its equation of state plays a pivotal role in understanding the thermodynamic properties of the core. However, uncertainties in experimental data have significant effects on the parameters within the iron equation of state. Using Bayesian statistical analysis coupled with Markov chain Monte Carlo (MCMC) simulation methods, we quantified the uncertainties in the equation of state parameters. During the simulation process, we proposed a simple yet efficient computational method for determining the probability of phase boundary data. The equation of state we obtained accurately reproduces various experimental data, including phase boundary experiments, static pressure data under different conditions, shock wave data, and sound velocity data at different states. With 100 posterior parameter samples, we predict that the density deficit of Earth's outer core falls within a range of approximately 8.7% to 9.7%, and the geodynamo power output due to latent heat release during the cooling and solidification of Earth's inner core is estimated to be between 0.458 to 6.002 terawatts.

1 Introduction

The Earth's core is primarily composed of iron, with minor inclusions of lighter elements such as nickel, sulfur, and oxygen (Li & Fei, 2014; Hirose et al., 2021). Iron significantly influences the propagation of seismic waves, and by meticulously analyzing these waves in conjunction with the equation of state for iron, we can deduce the spatial distribution of iron and other light elements within the core (Dziewoński & Anderson, 1981; Ichikawa et al., 2014; Kuwayama et al., 2020), thus revealing its complex structure. Additionally, the formation of the Earth's magnetic field is linked to the flow in the electrically conductive liquid outer core, a process driven by thermal convection (Labrosse, 2014; Singh et al., 2023a). Therefore, an in-depth study of the physical properties of iron under core conditions is of irreplaceable importance for elucidating the generation mechanism and evolutionary history of the Earth's magnetic field. Overall, investigating the thermodynamic behavior of iron under extreme high pressure is crucial for addressing fundamental questions about the Earth's core structure and dynamics; the precise equation of state for iron is key to these research topics.

Traditional methods for determining parameters in the equation of state model may introduce inaccuracies due to data uncertainty. Recognizing this is particularly important when studying the role of iron in the Earth's core. Although past studies have explored the equation of state for iron experimentally, they often did not utilize Bayesian data analysis, which incorporates prior knowledge and data uncertainty. Bayesian methods provide a probability distribution of parameters, continually updating it with new data, thus enhancing simulation accuracy and deepening our understanding of Earth's interior processes. In the Bayesian framework, conventional approaches determine phase transition boundaries based on Gibbs free energy but require complex numerical computations. To simplify this, Lindquist and Jadrich (Lindquist & Jadrich, 2022) introduced a model that categorized phase diagram data effectively. We focus on solving the phase boundary problem quickly and accurately, avoiding numerical inversion while adhering to the principle of equal Gibbs free energy between phases, significantly improving efficiency and accurately reproducing phase boundaries.

2 Simulation Methodology and Details

In data analysis, Bayesian statistics and Markov chain Monte Carlo (MCMC) methods are closely coupled to effectively manage uncertainty. Bayesian inference combines prior knowledge with new data to generate probabilistic distributions of model parameters, offering a more holistic perspective on uncertainty than traditional methods. In the study of multiphase equations, leveraging phase boundary data to constrain model parameters is an efficient approach, typically involving measurements of pressure (P) and temperature (T). Conventional methods are based on the principle of Gibbs free energy equilibrium and require numerical inversion to determine the relationship between P and T (P(T) or T(P)) for subsequent MCMC calculations of system state probabilities. However, this computational process is costly when dealing with complex inverse relationships between P and T. To enhance efficiency, Lindquist and Jadrich (Lindquist & Jadrich, 2022) innovatively transformed phase diagram data into a probability classification problem in their study of carbon's equation of state, achieving notable success. We also propose a simplified method that avoids complex numerical inversion while maintaining equal Gibbs free energy at phase boundaries. Specifically, we use probability estimates derived from indirect measurements to handle phase boundaries, rather than direct measurement-based probability computations, thus obtaining the P-T relationship without the need for numerical inversion, significantly improving computational efficiency. The details of our innovative phase boundary handling technique and parameter quantification can be found in the supplementary materials Text S2 and Text S3.

3 Multi-phase state equation of iron

In this study, we utilized the Python-emcee library (Foreman-Mackey et al., 2013) for parameter sampling, coupled with Python-numpy (Harris et al., 2020) for efficient data manipulation, and leveraged Python-seaborn (Waskom, 2021) to create visualizations, thereby facilitating in-depth analysis and intuitive representation of the data. Employing Bayesian theory and MCMC sampling techniques, we obtained a set of samples for the 40-dimensional parameters within the model (Dorogokupets, 2017). Through marginalization, we derived the marginal posterior distributions for each parameter, presenting them graphically to illustrate individual parameter behavior. Additionally, we computed and plotted a correlation matrix to visually depict inter-parameter relationships. Furthermore, based on 1000 sets of sample parameters, we estimated the parameter values corresponding to the maximum posterior probability (MPP). Detailed results can be found in the supplementary information Text S4.

The Fig.1 shows the phase diagram obtained using Maximum Posterior Probability (MPP) for parameter estimation. Along the isotherm at 300K, we calculate the bcc-hcp phase transition pressure to be 16.9 GPa. At a pressure of 0.1 MPa, the transformation temperatures from bcc(a) to fcc and from bcc(delta) to fcc are calculated to be 1190 K and 1611 K, respectively, with the melting point reaching 1801 K. We further computed the triple points where the bcc-fcc-liquid triple point is located at 6.0 GPa and 1994 K, the bcc-fcc-hcp triple point at 11.6 GPa and 774 K, and the fcc-hcp-liquid triple point at 109.5 GPa and 3698 K. Near the fcc-hcp-liquid triple point, our calculated phase boundary lines agree with the experimental data of Anzellini et al (Anzellini et al., 2013) and Morard et al (Morard et al., n.d.), but there is a discrepancy with the data of Sinmyo et al (Sinmyo et al., 2018). This mismatch may arise because our simulation dataset only included Morard's experimental data. In the high-pressure region, our calculated melting line for the hcp phase aligns with data based on ab initio free energy calculations (Alfè et al., 2002) and experimental data obtained by Li et al (Li et al., 2020). Additionally, the figure depicts the shock Hugoniot within the hcp phase, plotted using 100 sets of parameters, represented by thick black lines. The calculated shock curve intersects the melting line at the shock-induced melting point, which is located at 215 GPa and 5100 K. (The relationship between the shock wave and particle velocity used here is based on research by Brown (Brown et al., 2000).) .From the overall results, our calculated outcomes can accurately reproduce the phase boundary data and the shock Hugoniot within the hcp phase.

The Fig.2 displays the deviations between the pressure values calculated using MPP parameters for the various phases of iron (bcc, fcc, hcp, liquid) and the reference datasets.

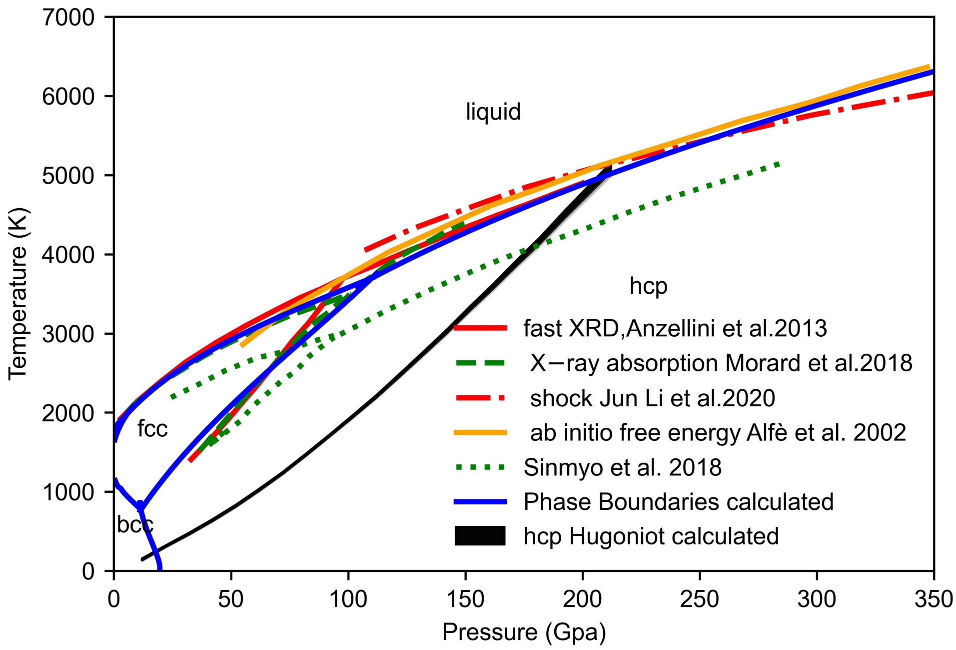

Figure 1. The figure presents a comparison of the calculated phase boundaries for iron obtained using maximum a posteriori parameter estimates against the reference boundary data(Anzellini et al., 2013; Morard et al., n.d.; Li et al., 2020; Alfè et al., 2002; Sinmyo et al., 2018). The black shaded area represents the shock curves within the hcp phase, computed using 100 sets of parameters; the relationship between the shock wave and particle velocity employed here is sourced from Brown (Brown et al., 2000).

.

For the Fe-bcc phase, based on experimental data (Zhang & Guyot, 1999; Dewaele et al., 2015; Dewaele & Garbarino, 2017; Liu et al., 2013; Shibazaki et al., 2016), the maximum deviation of our calculated results is less than 2 GPa. In the Fe-fcc phase, the maximum discrepancy between our computed pressure data and the experimental pressure data does not exceed 5 GPa (Nishihara et al., 2012; Shibazaki et al., 2020; Funamori et al., 1996; Anzellini et al., 2013; Komabayashi & Fei, 2010). Regarding the Fe-hcp phase, except for one set of anomalous data points (Tateno et al., 2010), the deviations of other data (Ohtani et al., 2013; Shahar et al., 2016; Sakai et al., 2014; Komabayashi et al., 2009; Yamazaki et al., 2012; Anzellini et al., 2013; González-Cataldo & Militzer, 2023) from our calculations are mostly within 10 GPa. However, some experimental data for the liquid phase (Kuwayama et al., 2020) show significant differences with the calculated results, which is likely due to substantial experimental errors. These experimental data were measured at multiple temperatures, not under isothermal conditions, and due to the density of the data, it is difficult to clearly label each temperature point on the graph.

The Fig.3 presents a comparison between the calculated shock-experiment-based pressures and the actual experimental measurements. Our calculations indicate that the onset of the shock melting curve for hcp iron occurs at a pressure of 215 GPa. However, the majority of empirical evidence suggests that the actual shock melting pressure is around 220 GPa. Therefore, Fig.3(a) focuses on the shock pressure range below 220 GPa, illustrating the deviation between the calculated shock pressure data and the experimentally determined pressure values within this range. As can be seen from the figure, these deviations are kept within 5 GPa, demonstrating a high degree of consistency between the our calculated results and experimental observations.To further understand the behavior of iron under extreme conditions, particularly in the fully molten state, Fig.3(b) provides a detailed comparison between computational and experimental data within the dynamic high-pressure range of 260 to 480 GPa. In this higher pressure interval, most of the data deviations are still maintained below 10 GPa, indicating that even under very high dynamic pressures, our computational data maintains good agreement with the experimental data (Brown & Mcqueen, 1986; Brown et al., 2000; W. W. Anderson & Ahrens, 1994; Li et al., 2020), thereby validating the accuracy and reliability of our computational results. Synthesizing these findings, our equations of state obtained through MPP parameter estimations are capable of effectively replicating the pressure characteristics of iron across a considerable range.

The Fig.4(a) demonstrates that at room temperature conditions (300 K), the calculated bulk wave speeds in the hexagonal close-packed (hcp) structure across various pressures (30-170 GPa) are higher relative to Murphy's experimental data (Murphy et al., 2013), yet within this pressure range, we also identified that Ohtani's longitudinal wave speed experimental data (Ohtani et al., 2013) are consistently higher than Murphet's measurements. Fig.4(b) shows that within this temperature range, our computed sound velocity data exhibit good agreement with Kuwayama's experimental results (Kuwayama et al., 2020) from High-pressure inelastic x-ray scattering (IXS) measurements of liquid iron. Moreover, when comparing our shock-induced high-pressure acoustic speeds to the findings of Anderson's research (W. W. Anderson & Ahrens, 1994), our calculations reveal a maximum deviation of less than 6.6%, thus confirming the consistency and accuracy of our work.

Furthermore, in the supplementary material Text S5 section, this study compares a series of experimental measurements of physical properties with the results calculated from 100 parameter samples derived from posterior distribution sampling. Our computational findings indicate that the heat capacity of the body-centered cubic (bcc) structure is largely consistent with the experimental data reported by Desai (Desai, 1986). However, at the Curie temperature of 1043 K, the experimentally measured heat capacity significantly exceeds our computational results, which may be attributed to an insufficient model description of the ferromagnetic transition process. Regarding the ther-

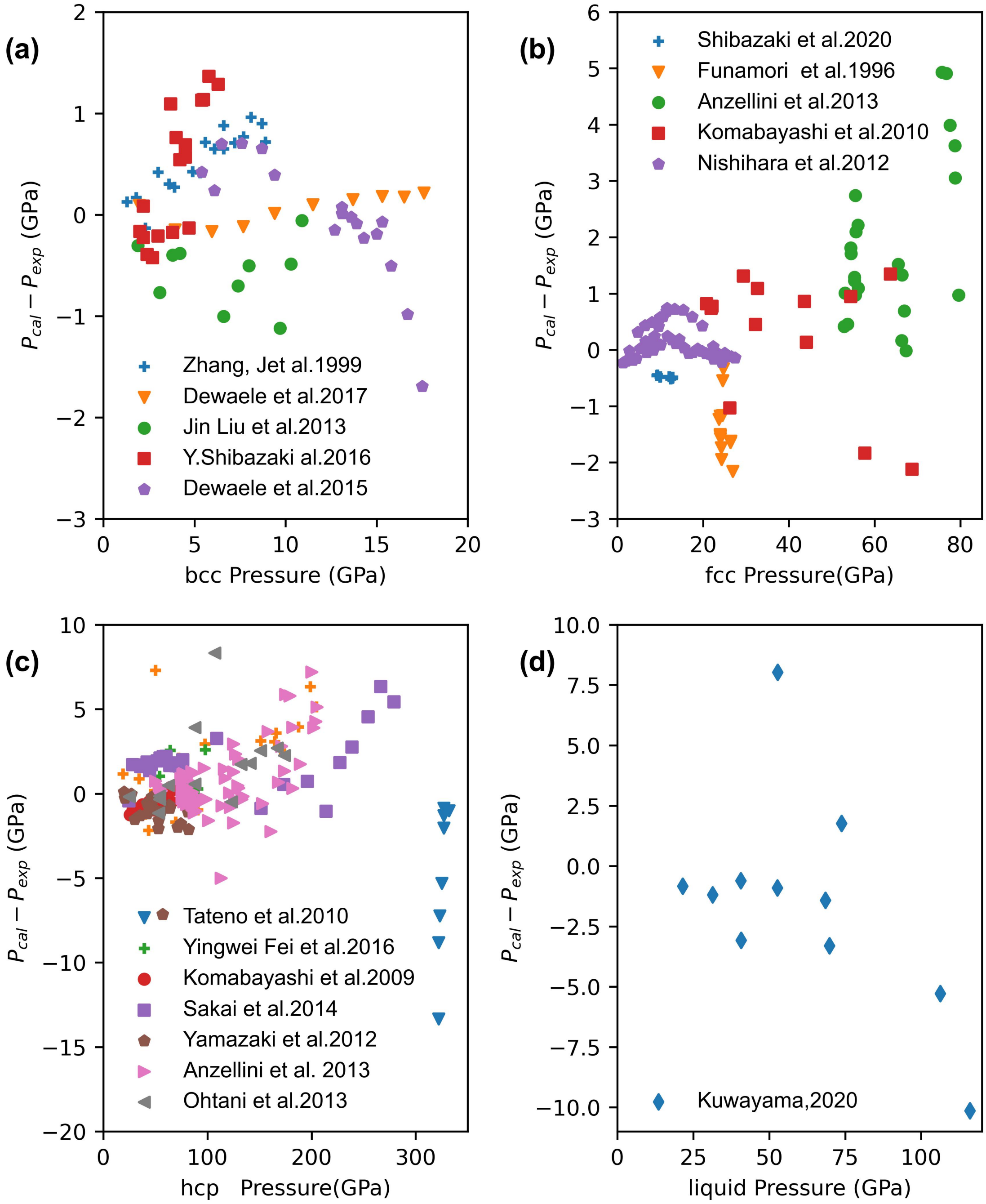

Figure 2. The Fig.2 illustrates the discrepancies between the pressure values computed utilizing MPP parameters applied to various phases of Iron - bcc (a), fcc (b), hcp (c), Liquid (d) - and corresponding reference static high pressure data sets.

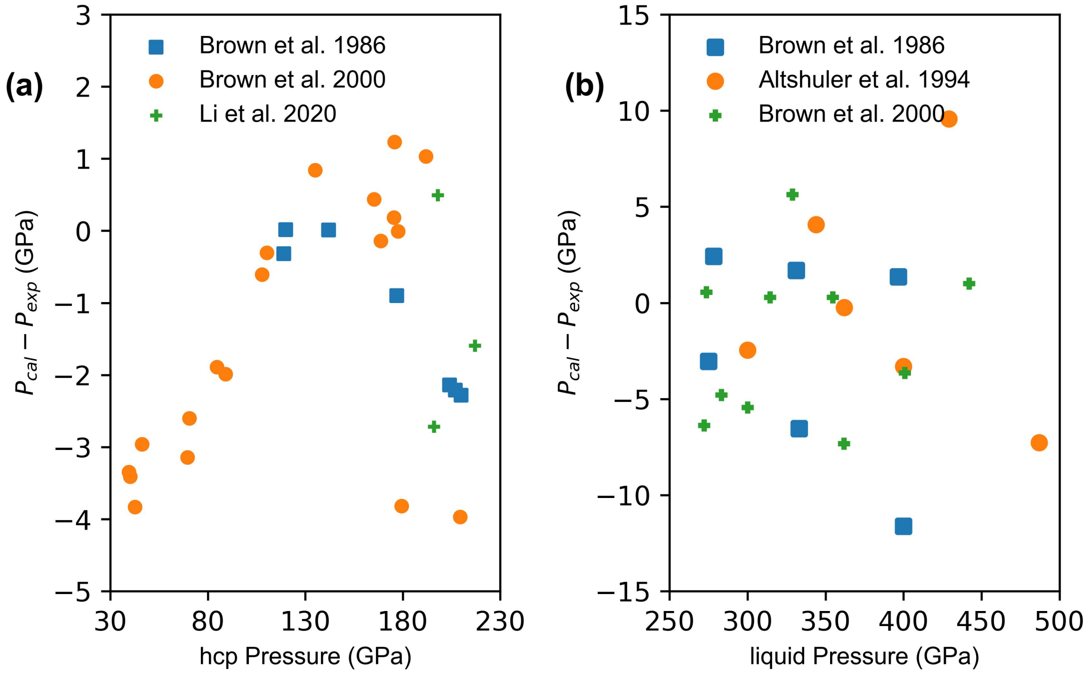

Figure 3. The picture we use MPP parameters estimation to calculate the differences between the computed dynamic high-pressure data for the hcp phase and the liquid phase, and compare them with the corresponding shock experimental data (Brown & Mcqueen, 1986; Brown et al., 2000; W. W. Anderson & Ahrens, 1994; Li et al., 2020).

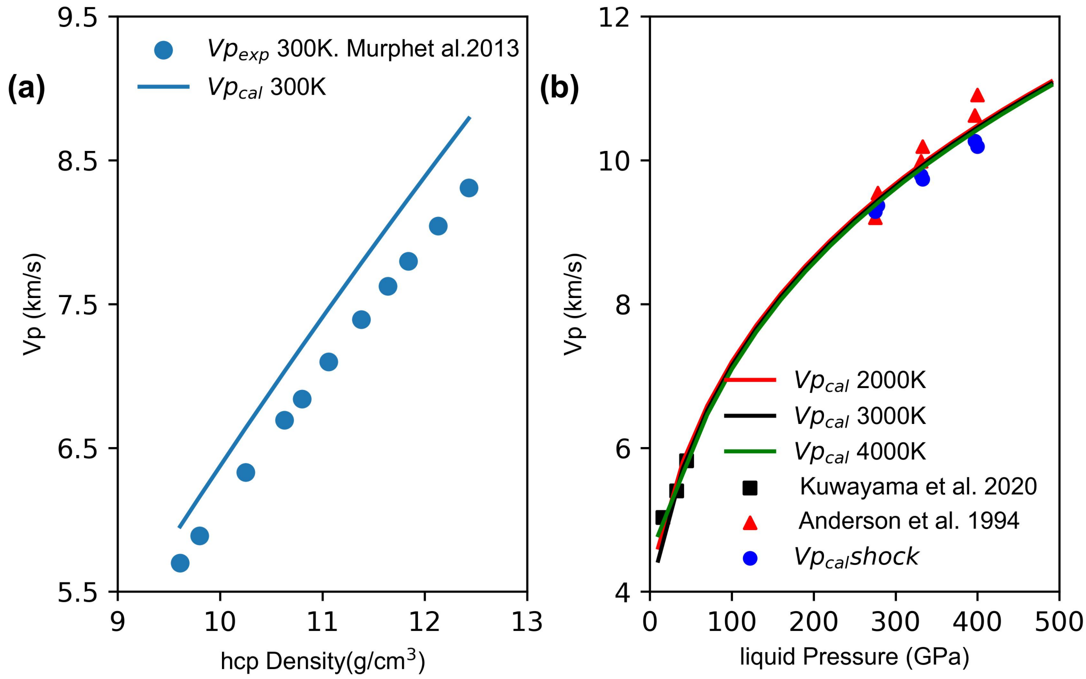

Figure 4. In figure (a), the blue solid line indicates the bulk sound speed of hcp-iron at 300K as calculated by us, and the corresponding blue dots represent experimental data from Murphy (Murphy et al., 2013).In the figure (b), solid lines show our calculated sound speeds at 2000K, 3000K, and 4000K. Black squares are IXS experimental data (Kuwayama et al., 2020); red triangles, shock experiment data (W. W. Anderson & Ahrens, 1994); and blue circles, corresponding shock calculation results.

mal expansion coefficient of iron in bcc and face-centered cubic (fcc) structures, our calculations are in agreement with the experimental data from Dorogokupets's supplementary materials (Dorogokupets, 2017) at lower temperatures; however, at higher temperatures, the computed values are slightly below the experimental observations, possibly due to inadequate experimental constraints applied during the simulation phase. Concerning the isothermal pressure curves of solid phases, our computational results demonstrate that the pressure curves for bcc-Fe at 15 K and 300 K, as well as fcc-Fe at 1073 K and 1273 K, and hcp-Fe at various temperatures, closely match the experimental data (Dewaele & Garbarino, 2017; Liu et al., 2013; Nishihara et al., 2012; Fei et al., 2016). Similar to the heat capacity calculations, the uncertainty range of the isothermal pressure curves is relatively small.

Overall, by utilizing Bayesian statistical theory and MCMC sampling methods, we have systematically obtained the uncertainties of the parameters in iron's equation of state. The simulation results effectively model the diverse behaviors of iron under various conditions of pressure, volume, and temperature, including heat fusion and thermal expansion at ambient pressure as temperatures change, pressure variations at different temperatures, and performance during shock experiments and phase boundary transitions. We achieved equation of state predictions for pressures that cover the range of the Earth's core, with subsequent presentation of our predictions for the thermodynamic properties of the Earth's core to follow.

4 Applications under the Earth core conditions

To accurately quantify certain thermodynamic properties of the Earth's core, we selected 100 sets of sample parameters to assess the uncertainty range in predicted physical quantities introduced by calibration data errors through simulation calculations.

In the simulation study, we have conducted calculations on the melting characteristics of pure iron under conditions at the Earth's Inner Core Boundary (ICB), where at a pressure of 330 GPa, the theoretical melting temperature range for pure iron is between 5997 K and 6262 K. However, the actual melting temperature in the core might be lower due to the presence of lighter elements. To validate these computational results against geological experimental data, we plotted the density(ρ), sonic velocity(V_P), and shear modulus(K_S) of liquid pure iron at various temperatures (4000 K, 5000 K, and 6000 K) under ICB pressure, comparing them with data from the Preliminary Reference Earth Model (PREM) (Dziewoński & Anderson, 1981). The relevant details are shown in the Fig.5. The solid-liquid phase transition temperatures (at the CMB) computed by us spanned intervals of (2928 K-3086 K), (3621 K-3795 K), and (4297 K-4479 K). When setting T_{ICB} at 5000 K, this upper limit approximates the 3800 K proposed by Brown and McQueen in 1986 (Brown & Mcqueen, 1986), as well as the 3739 K given by Stacey and Davis in 2004 (Stacey & Davis, 2004). Adopting a value of 4676 K yields a CMB temperature range of (3398 K-3568 K), which aligns closely with Anderson's 3637 K and Ichikawa's 3585 K (Ichikawa et al., 2014).

Assuming T_{ICB} to be 5000 K, the estimated densities of liquid iron at the CMB and ICB conditions are respectively (10.854 g/cm^3- 10.786 g/cm^3) and (13.226 g/cm^3 - 13.348 g/cm^3). Moreover, the graphs reveal that both the sonic velocity and shear modulus exhibit relatively low sensitivity to temperature changes; our computations show that the outer core's values in these two physical parameters are nearly consistent with PREM data, with small discrepancies in sonic velocity. The figures also demonstrate that the difference in density between solid and liquid iron $\Delta\rho_{solid}$ at the ICB is less than the density change resulting from internal state variations within liquid iron $\Delta\rho_{liquid}$, suggesting compositional differences between the inner and outer cores. Nevertheless, the calculated density deviation range for the outer core (8.7% to 9.7%) provides a strong constraint on the content of light elements.

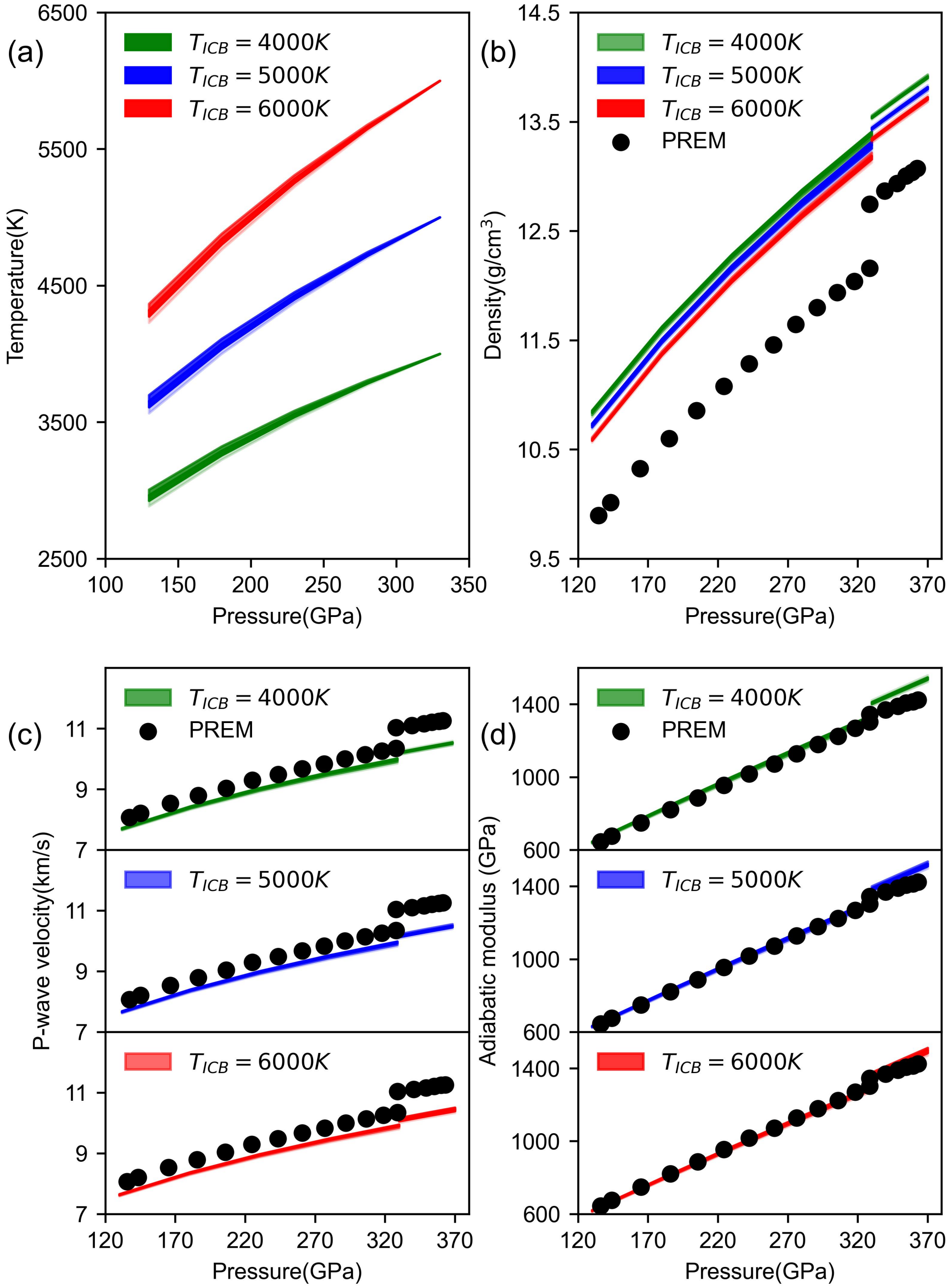

Figure 5. A comparison of the physical properties of liquid iron and hcp-iron, calculated based on an isentropic temperature profile, is conducted in conjunction with the PREM (Dziewoński & Anderson, 1981) data. Calculated isentropic temperature profile (a). Calculated density along the T_{ICB} isentrope (b). Calculated P-wave velocity along the isentrope (c). Calculated adiabatic bulk modulus along adiabats for solid and liquid iron (d). (When T_{ICB} takes the values of 4000 K, 5000 K, and 6000 K respectively)

The latent heat of fusion ($\Delta\ H_m$) released during the solidification of iron at the Earth's Inner Core Boundary plays a critical role in driving external convection in the core, contributing approximately 20% to the total energy. Based on the newly calculated latent heat of fusion for iron under ICB conditions-(0.526-0.973 kJ/g) -we re-evaluated the total energy released during Earth's core cooling process and its corresponding power output. Multiplying this latent heat by the mass of the core, estimated to be around 1.1 $\times\ 10^{23}$ kg, results in a total energy release of 8.987×10^{2} joules. Considering the shortest (0.565 billion years) and longest (4 billion years) estimates for the age of the core, and converting these durations into seconds, we further derived the power output range across these timescales: at the shortest time scale, the power output is approximately 3.244-6.002 TW, while at the longest time scale, it reduces to about 0.458-0.848 TW. This lower bound of the power output is essentially consistent with the results obtained by Singh (Singh et al., 2023b). These calculations provide a rough yet significant estimate, indicating that even over vast geological timescales, the Earth's core cooling process continuously releases enormous amounts of energy, which significantly sustains the operation of the geodynamo.

5 Conclusions

In this paper, we perform uncertainty quantization for parameters up to 40 dimensions in the multiphase iron equation of state based on Bayesian theory and MCMC sampling. When handling phase boundary data, we employ probability estimates derived from indirect measurements in lieu of direct measurement-based probability computations, allowing us to obtain the functional relationship between pressure and temperature without resorting to numerical inversion, significantly enhancing computational efficiency. The uncertainty quantization results of the parameters in the iron multiphase equation of state can not only reproduce the pressure, thermal fusion, modulus and expansion coefficient well, but also reproduce the phase diagram information and impact temperature data well. Under the assumption of an Inner Core Boundary (ICB) temperature of 5000 K, we have computed the range of density variation of liquid iron in the outer core region to be between 8.7% to 9.7%. This precise density differential data effectively constrains the estimation of possible light element content within the outer core. Furthermore, we have also reassessed the contribution to geomagnetic dynamo output power resulting from latent heat release during Earth's inner core cooling and solidification process, estimating this figure to fall within the interval of 0.458 to 6.002 TW. This body of research findings holds significant implications for advancing our understanding of the evolutionary history of the Earth's core.

Open Research Section

Data used in this study are available through the following sources:(Li et al., 2020; Morard et al., n.d.; O. L. Anderson, 1986; Kaufman et al., 1963; Johnson et al., 1962; Zhang & Guyot, 1999; Dewaele et al., 2015; Dewaele & Garbarino, 2017; Liu et al., 2013; Shibazaki et al., 2016; Nishihara et al., 2012; Shibazaki et al., 2020; Funamori et al., 1996; Anzellini et al., 2013; Komabayashi & Fei, 2010; Ohtani et al., 2013; Shahar et al., 2016; Sakai et al., 2014; Komabayashi et al., 2009; Yamazaki et al., 2012; González-Cataldo & Militzer, 2023; Kuwayama et al., 2020; Brown & Mcqueen, 1986; Brown et al., 2000; W. W. Anderson & Ahrens, 1994; Desai, 1986)

Acknowledgments

This work was supported by the National Key R&D Program of China (Grant No. 2021YFB3802300), the National Nature Science Foundation of China (Grant Nos. 12372370).

References

Alfè, D., Price, G. D., & Gillan, M. J. (2002, Apr). Iron under earth's core conditions: Liquid-state thermodynamics and high-pressure melting curve from ab initio calculations. *Phys. Rev. B*, *65*, 165118. Retrieved from https://link.aps.org/doi/10.1103/PhysRevB.65.165118 doi: 10.1103/PhysRevB.65.165118

Anderson, O. L. (1986). Properties of iron at the earth's core conditions. *Geophysical Journal International*, *84*, 561-579. Retrieved from https://api.semanticscholar.org/CorpusID:128695991

Anderson, W. W., & Ahrens, T. (1994). An equation of state for liquid iron and implications for the earth's core. *Journal of Geophysical Research*, *99*, 4273-4284. Retrieved from https://api.semanticscholar.org/CorpusID:27551780

Anzellini, S., Dewaele, A., Mezouar, M., Loubeyre, P., & Morard, G. (2013). Melting of iron at earth's inner core boundary based on fast x-ray diffraction. *Science*, *340*, 464 - 466. Retrieved from https://api.semanticscholar.org/CorpusID:31604508

Brown, J. M., Fritz, J. N., & Hixson, R. S. (2000). Hugoniot data for iron. *Journal of Applied Physics*, *88*, 5496-5498. Retrieved from https://api.semanticscholar.org/CorpusID:121588362

Brown, J. M., & Mcqueen, R. G. (1986). Phase transitions, grüneisen parameter, and elasticity for shocked iron between 77 gpa and 400 gpa. *Journal of Geophysical Research*, *91*, 7485-7494. Retrieved from https://api.semanticscholar.org/CorpusID:129107803

Desai, P. D. (1986). Thermodynamic properties of iron and silicon. *Journal of Physical and Chemical Reference Data*, *15*, 967-983. Retrieved from https://api.semanticscholar.org/CorpusID:95590422

Dewaele, A., Denoual, C., Anzellini, S., Occelli, F., Mezouar, M., Cordier, P., … Rausch, E. (2015, May). Mechanism of the $\alpha - \epsilon$ phase transformation in iron. *Phys. Rev. B*, *91*, 174105. Retrieved from https://link.aps.org/doi/10.1103/PhysRevB.91.174105 doi: 10.1103/PhysRevB.91.174105

Dewaele, A., & Garbarino, G. (2017). Low temperature equation of state of iron. *Applied Physics Letters*, *111*, 021903. Retrieved from https://api.semanticscholar.org/CorpusID:103212786

Dorogokupets, P. I. e. a. (2017). Thermodynamics and equations of state of iron to 350 gpa and 6000 k. *Scientific Reports*, *7*, 41863. doi: 10.1038/srep41863

Dziewoński, A. M., & Anderson, D. L. (1981). Preliminary reference earth model. *Physics of the Earth and Planetary Interiors*, *25*, 297-356. Retrieved from https://api.semanticscholar.org/CorpusID:129232713

Fei, Y., Murphy, C. A., Shibazaki, Y., Shahar, A., & Huang, H. (2016). Thermal equation of state of hcp-iron: Constraint on the density deficit of earth's solid inner core. *Geophysical Research Letters*, *43*, 6837 - 6843. Retrieved from https://api.semanticscholar.org/CorpusID:132866914

Foreman-Mackey, D., Hogg, D. W., Lang, D., & Goodman, J. (2013, March). emcee: The MCMC Hammer. , *125*(925), 306. doi: 10.1086/670067

Funamori, N., Yagi, T., & Uchida, T. (1996). High-pressure and high-temperature in situ x-ray diffraction study of iron to above 30 gpa using ma8-type apparatus. *Geophysical Research Letters*, *23*, 953-956. Retrieved from https://api.semanticscholar.org/CorpusID:128619359

González-Cataldo, F., & Militzer, B. (2023). Ab initio determination of iron melting at terapascal pressures and super-earths core crystallization. *Physical Review Research*. Retrieved from https://api.semanticscholar.org/CorpusID:262178924

Harris, C. R., Millman, K. J., van der Walt, S. J., Gommers, R., Virtanen, P., Cournapeau, D., … Oliphant, T. E. (2020, September). Array programming with

NumPy. *Nature*, *585*(7825), 357–362. Retrieved from https://doi.org/10.1038/s41586-020-2649-2 doi: 10.1038/s41586-020-2649-2

Hirose, K., Wood, B. J., & Voadlo, L. (2021). Light elements in the earth's core. *Nature Reviews Earth & Environment*, *2*, 645 - 658. Retrieved from https://api.semanticscholar.org/CorpusID:237272150

Ichikawa, H., Tsuchiya, T., & Tange, Y. (2014). The p-v-t equation of state and thermodynamic properties of liquid iron. *Journal of Geophysical Research: Solid Earth*, *119*, 240 - 252. Retrieved from https://api.semanticscholar.org/CorpusID:130604173

Johnson, P. C., Stein, B. A., & Davis, R. S. (1962). Temperature dependence of shock-induced phase transformations in iron. *Journal of Applied Physics*, *33*, 557-561. Retrieved from https://api.semanticscholar.org/CorpusID:120137987

Kaufman, L., Clougherty, E. V., & Weiss, R. J. (1963). The lattice stability of metals*iii*. iron. *Acta Metallurgica*, *11*, 323-335. Retrieved from https://api.semanticscholar.org/CorpusID:94888216

Komabayashi, T., & Fei, Y. (2010). Internally consistent thermodynamic database for iron to the earth's core conditions. *Journal of Geophysical Research*, *115*, 1-12. Retrieved from https://api.semanticscholar.org/CorpusID:54919859

Komabayashi, T., Fei, Y., Meng, Y., & Prakapenka, V. B. (2009). In-situ x-ray diffraction measurements of the γ-ϵ transition boundary of iron in an internally-heated diamond anvil cell. *Earth and Planetary Science Letters*, *282*, 252-257. Retrieved from https://api.semanticscholar.org/CorpusID:130768562

Kuwayama, Y., Morard, G., Nakajima, Y., Hirose, K., Baron, A. Q., Kawaguchi, S. I., … Ohishi, Y. (2020). Equation of state of liquid iron under extreme conditions. *Physical review letters*, *124 16*, 165701. Retrieved from https://api.semanticscholar.org/CorpusID:218562532

Labrosse, S. (2014). Thermal evolution of the core with a high thermal conductivity. *Physics of the Earth and Planetary Interiors*, *247*, 36-55. Retrieved from https://api.semanticscholar.org/CorpusID:122507563

Li, J., & Fei, Y. (2014). Experimental constraints on core composition.. Retrieved from https://api.semanticscholar.org/CorpusID:92064071

Li, J., Wu, Q., Li, J., Xue, T., Tan, Y., Zhou, X., … Sekine, T. (2020). Shock melting curve of iron: A consensus on the temperature at the earth's inner core boundary. *Geophysical Research Letters*, *47*. Retrieved from https://api.semanticscholar.org/CorpusID:225363462

Lindquist, B. A., & Jadrich, R. B. (2022). Uncertainty quantification for a multiphase carbon equation of state model. *Journal of Applied Physics*. Retrieved from https://api.semanticscholar.org/CorpusID:248331170

Liu, J., Lin, J., Alatas, A., & Bi, W. (2013). Sound velocities of bcc-fe and fe0.85si0.15 alloy at high pressure and temperature. *Physics of the Earth and Planetary Interiors*, *233*, 24-32. Retrieved from https://api.semanticscholar.org/CorpusID:21680558

Morard, G., Boccato, S., Rosa, A. D., Anzellini, S., Miozzi, F., Henry, L., … Torchio, R. (n.d.). Solving controversies on the iron phase diagram under high pressure. *Geophysical Research Letters*, *45*, 11,074 - 11,082. Retrieved from https://api.semanticscholar.org/CorpusID:92985762

Murphy, C. A., Jackson, J. M., & Sturhahn, W. (2013). Experimental constraints on the thermodynamics and sound velocities of hcp-fe to core pressures. *Journal of Geophysical Research: Solid Earth*, *118*, 1999 - 2016. Retrieved from https://api.semanticscholar.org/CorpusID:28881426

Nishihara, Y., Nakajima, Y., Akashi, A., Tsujino, N., Takahashi, E., Funakoshi, K., & Higo, Y. (2012). Isothermal compression of face-centered cubic iron. *American Mineralogist*, *97*, 1417 - 1420. Retrieved from https://api.semanticscholar.org/CorpusID:54601004

Ohtani, E., Shibazaki, Y., Sakai, T., Mibe, K., Fukui, H., Kamada, S., … Baron, A. Q. (2013). Sound velocity of hexagonal close-packed iron up to core pressures. *Geophysical Research Letters*, *40*, 5089 - 5094. Retrieved from https://api.semanticscholar.org/CorpusID:128586157

Sakai, T., Takahashi, S., Nishitani, N., Mashino, I., Ohtani, E., & Hirao, N. (2014). Equation of state of pure iron and fe0.9ni0.1 alloy up to 3mbar. *Physics of the Earth and Planetary Interiors*, *228*, 114-126. Retrieved from https://api.semanticscholar.org/CorpusID:129344647

Shahar, Anat, Murphy, Caitlin, Fei, Yingwei, … Yuki (2016). Thermal equation of state of hcp-iron: Constraint on the density deficit of earth's solid inner core. *Geophysical Research Letters*, *43*(13), 6837-6843.

Shibazaki, Y., Nishida, K., Higo, Y., Igarashi, M., Tahara, M., Sakamaki, T., … Ohtani, E. (2016). Compressional and shear wave velocities for polycrystalline bcc-fe up to 6.3 gpa and 800 k. *American Mineralogist*, *101*, 1150 - 1160. Retrieved from https://api.semanticscholar.org/CorpusID:101475614

Shibazaki, Y., Nishida, K., Tobe, H., Terasaki, H., & Higo, Y. (2020). Effect of hydrogen on the sound velocity of fcc-fe at high pressures and high temperatures.. Retrieved from https://api.semanticscholar.org/CorpusID:222954715

Singh, S., Briggs, R., Gorman, M. G., Benedict, L. X., Wu, C. J., Hamel, S., … Smith, R. F. (2023a). A structural study of hcp and liquid iron under shock compression up to 275 gpa.. Retrieved from https://api.semanticscholar.org/CorpusID:258180169

Singh, S., Briggs, R., Gorman, M. G., Benedict, L. X., Wu, C. J., Hamel, S., … Smith, R. F. (2023b). Structural study of hcp and liquid iron under shock compression up to 275 gpa. *Physical Review B*. Retrieved from https://api.semanticscholar.org/CorpusID:265190891

Sinmyo, R., Hirose, K., & Ohishi, Y. (2018). Melting curve of iron to 290 gpa determined in a resistance-heated diamond-anvil cell. *Earth and Planetary Science Letters*. Retrieved from https://api.semanticscholar.org/CorpusID:134890949

Stacey, F. D., & Davis, P. (2004). High pressure equations of state with applications to the lower mantle and core. *Physics of the Earth and Planetary Interiors*, *142*, 137-184. Retrieved from https://api.semanticscholar.org/CorpusID:129634838

Tateno, S., Hirose, K., Ohishi, Y., & Tatsumi, Y. (2010). The structure of iron in earth's inner core. *Science*, *330*, 359 - 361. Retrieved from https://api.semanticscholar.org/CorpusID:206528628

Waskom, M. L. (2021). seaborn: statistical data visualization. *Journal of Open Source Software*, *6*(60), 3021. Retrieved from https://doi.org/10.21105/joss.03021 doi: 10.21105/joss.03021

Yamazaki, D., Ito, E., Yoshino, T., Yoneda, A., Guo, X., Zhang, B., … Funakoshi, K. (2012). P-v-t equation of state for ϵ-iron up to 80 gpa and 1900 k using the kawai-type high pressure apparatus equipped with sintered diamond anvils. *Geophysical Research Letters*, *39*. Retrieved from https://api.semanticscholar.org/CorpusID:129695765

Zhang, J., & Guyot, F. (1999). Thermal equation of state of iron and fe0.91si0.09. *Physics and Chemistry of Minerals*, *26*, 206-211. Retrieved from https://api.semanticscholar.org/CorpusID:97322900